CrystEngComm

Accepted Manuscript

ROYAL SOCIETY OF CHEMISTRY

www.rsc.org/crystengcomm

Journal Name

ARTICLE

Electrochemical and chemical insertion/deinsertion of magnesium in spinel-type $MgMn_2O_4$ and lambda-MnO_2 for both aqueous and non-aqueous magnesium-ion batteries

Received 00th January 20xx,
Accepted 00th January 20xx

DOI: 10.1039/x0xx00000x

www.rsc.org/

M. Cabello, R. Alcántara, F. Nacimiento, G. Ortiz, P. Lavela and J. L. Tirado

By both chemical and electrochemical ways, magnesium has been reversibly removed from $MgMn_2O_4$ (s.g. $I4_1/amd$) with appropiate texture to form single-phase and nanocrystalline λ-MnO_2 (s.g. Fd-3m). Cubic λ-MnO_2 is not stable after annealing in both air and Ar atmosphere. The oxidation of Mn(III) to Mn(IV) eliminates the tetragonal distortion of the spinel-type lattice, but λ-MnO_2 is more effectively obtained when powdered $MgMn_2O_4$ has large specific surface area and small particle size. In aqueous solution of magnesium salt, λ-MnO_2 is formed by galvanostatic charge of $MgMn_2O_4$ and continuous Ar-flowing for removing oxygen from the solution. Starting from λ-MnO_2, the tetragonal structure of $MgMn_2O_4$ and the cubic structure of $LiMn_2O_4$ are generated by electrochemical cycling in aqueous solutions containing salts of magnesium and lithium, respectively. In aqueous solution cell, this material exhibits a reversible capacity of about 150 mAh g^{-1} and can be used in magnesium-ion batteries demonstrating to be competitive against the lithium counterparts. In the absence of metallic Mg, the use of carbonate-bases solvents can be a good choice for veritable non-aqueous magnesium-ion batteries, for example using positive electrode materials like $MgMn_2O_4$ (magnesium-ion source) and negative eletrode materials like V_2O_5. In non-aqueous solvents (ethylene carbonate-diethyl carbonate mixture) the cubic phase λ-MnO_2 is not formed, the tetragonal structure of $Mg_xMn_2O_4$ is preserved and its lattice cell is contracted.

1. Introduction

The insertion of polivalent cations (Mg^{2+}, Ca^{2+}, Al^{3+} and others) offers the advantage of charging two (or three) electrons per ion to the host material, and this fact may drive to develop high-energy batteries which would be competitive against lithium-ion batteries and other systems that use monovalent ions.[1] Thus, several compounds have been proposed for reversible accommodation of magnesium in their frameworks, such as MnO_2, Mo_6S_8 and V_2O_5.[2] However, the polyvalent ions use to be strongly bonded to the host solid and the extraction process is slow. Although it is generally believed that the diffusion of magnesium ions in host materials is slow, however, based on calculations, Ling and Musino reported that the mobility of Mg^{2+} in compounds such as $MgMn_2O_4$ can be comparable to that of Li^+ in typical Li-ion battery.[3]

Several phases of MnO_2 such as hollandite, todorokite, birnessite and spinel-type λ-MnO_2 can intercalate magnesium ions, but the retention of the capacity upon charge/discharge cycling is usually poor. Recently, Zhang et al. proposed that the magnesiation process of α-MnO_2 proceeds by conversion-type reaction on the surface of the MnO_2 particles rather than intercalation reaction.[4] Besides the intrinsic properties of MnO_2, it may be that some part of the irreversibility and capacity fade observed for MnO_2 batteries could be produced by the incompatibility between the metallic Mg electrode and the electrolyte solution.

A key aspect for developing batteries is to select a suitable electrolyte, and both aqueous and non-aqueous electrolytes have been studied for magnesium batteries.[5] Metallic magnesium cannot be used in the presence of carbonates solvents, such as propylene carbonate (PC), ethylene carbonate (EC) and diethyl carbonate (DEC), because the electrodeposition of Mg is impossible in these solvents. Acetonitrile (AN) is more compatible than carbonates, but the cycling behaviour is still poor. PhMgCl-$AlCl_3$ (Grygnard-type compound) in tetrahydrofurane (THF) solution form acidic species that dissolve surface films and reversible dissolution/electrodeposition of magnesium can be achieved, but this solution can corrode the stainless steel used like current collector in the battery. In solutions of THF containing PhMgCl and $AlCl_3$, Yagai et al. observed pitting corrosion on the surfaces of Cu, Ni, stainless steel, Ti, and Al electrodes after the first anodic polarization from 0 to 4 V.[6] It would be preferred to use Pt, glassy carbon and graphite as current collectors, substrate of electrode active material and battery case, but this solution seems unfeasible for commercial batteries.

In this work we have explored and optimized the experimental conditions to reversibly remove magnesium from $MgMn_2O_4$. For this purpose, firstly $MgMn_2O_4$ was prepared at

Department of Inorganic Chemistry, Campus of Rabanales, University of Cordoba, 14071 Córdoba, Spain.
E-mail: iq2alror@uco.es; Fax: +34 957218621
Supplementary Information (ESI) available: [details of any supplementary information available should be included here]. See DOI: 10.1039/x0xx00000x

several temperatures. The obtained samples have different microstructure and texture properties that influence on the possibility of achieving demagnesiation to form λ-MnO_2. Finally, we have studied the electrochemical behaviour of this material as electrode for magnesium-ion batteries in both aqueous and non-aqueous batteries, and we have found that it can be competitive against lithium.

2. Experimental

2.1 Preparation of $MgMn_2O_4$

$MgMn_2O_4$ was prepared following the method of Pechini. Citric acid and ethylene glycol were added to an aqueous solution 0.5 M in $Mg(NO_3)_2.6H_2O$ and 0.25 M in $Mn(NO_3)_2.4H_2O$ to yield the molar ratios magnesium:manganese:citric acid:ethylene glycol=0.5:1.0:3.0:9.0. The solution was heated to about 70°C to remove water while mechanical stirring was applied. The resulting rubbery polymer was transferred to a high-form crucible of alumina and heated to 200°C overnight. The obtained powder was ground in an agate mortar and then heated to 400, 550 or 800°C for ten hours.

2.2 Chemical conversion of $MgMn_2O_4$ to λ-MnO_2

To obtain λ-MnO_2, 0.4 g of $MgMn_2O_4$ were put in a beaker with about 140 mL of nitric acid solution at pH 2, under continuous stirring for 50 minutes. The solution pH was monitored and stabilized at ca. 2.0. After the acid treatment, the solid was separated by centrifugation, washed with deionized water and dried under vacuum at 90°C.

2.3 Characterization methods

XRD measurements were carried out in a Bruker D8-Advance instrument with CuKα1 radiation. In the case of the XRD patterns of electrodes supported on Ti substrate, the Bragg reflections of Ti were used for calibration. In-situ XRD patterns of λ-MnO_2 were collected at several temperatures in a Bruker D8-Advance instrument equipped with a furnace Anton Paar HTK1200N.

FTIR spectra were obtained by transmission mode in a FT-MIR Bruker Tensor 27 spectrophotometer. The spectra were recorded on pellets prepared by diluting the samples with KBr.

Isotherms of nitrogen adsorption were recorded in a Quantachrome instrument at the temperature of liquid nitrogen. The samples were previously outgassed under dynamic vacuum. The isotherms were used to calculate the specific surface area using the Brunauer–Emmett–Teller theory (BET), while the pore size distribution, the average pore size and the total pore volume were calculated by applying the formulism of Barrett-Joyner-Halenda (BJH) to the desorption branch.

To study the microstructure of the particles a Transmission Electron Microscope (TEM) JEM1400 instrument was used.

Differential scanning calorimetry (DSC) measurements were recorded in a Calisto Labsys Evo instrument at 10°C/min of heating rate and using alumina pans.

2.4 Electrochemical experiments

The electrochemical experiments were performed in a multichannel VMP instrument.

Electrochemical tests in aqueous solution were carried out in beaker cell, with Pt as the counter electrode and Ag/AgCl as reference electrode. The working electrode was a mixture of active material:carbon black:binder=80:10:10 supported on Ti substrate. The carbon black sample was supplied by SAFT. The electrode mass charge was 2.1-3.7 mg cm^{-2}. The electrolyte solution was 100 mL of 3 M $Mg(NO_3)_2$. The electrolyte aqueous solution was degassed by flowing Ar at a rate of 70 ml min^{-1}.

For non-aqueous batteries, Swagelok-type cells were mounted in an M-Braun glove-box filled with Ar. The positive electrode was a mixture of active material ($MgMn_2O_4$, 80%), carbon black (10%) and binder (PVDF, 10%) on Pt substrate. The electrolyte solution was 0.5 M $Mg(ClO_4)_2$ in EC:DEC (50:50). Pt was used like reference electrode. The negative electrode was a mixture of active material (V_2O_5, 80%), carbon black (10%) and binder (10%).

3. Results and discussion

3.1 Microstructure and texture analysis

The only phase observed in the samples obtained after annealing the precursor at 400 and 550°C is nanocrystalline $MgMn_2O_4$, and the corresponding XRD patterns can be indexed in the space group $I4_1/amd$ (Fig. 1). The average grain size values of this phase obtained from Scherrer equation for 400, 550 and 800°C are 17.2, 24.3 and 93.6 nm, respectively. At 800°C the occurrence of the minor phase Mg_6MnO_8 is also detected. In the TEM micrographs, it is observed that the particle size tends to increase with the annealing temperature.

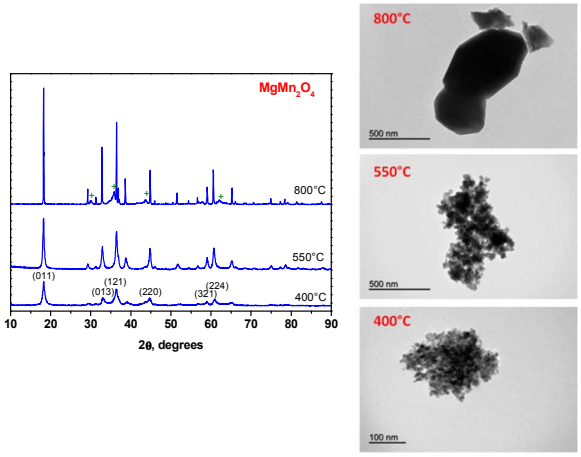

Fig. 1 XRD patterns and TEM micrographs for $MgMn_2O_4$ (JCPDS:23-0392) prepared at 400, 550 and 800°C. The Miller indexes are given (s.g. $I4_1/amd$). The Bragg peaks of the impurity $MgMn_6O_8$ (JCPDS:11-0031) are marked with a green cross (+).

From 400 to 550°C there is a substantial change in the texture, surface area and porosity (Fig. 2 and Table 1). The adsorption isotherm of the sample prepared at 400°C exhibits a hysteresis loop of type H4 which can be associated with a

complex material containing both micropores and mesopores. For the sample annealed at 550°C, the observed inverse type H2 hysteresis loop can be associated with the occurrence of pore blocking, and this hysteresis type was previously observed in materials where the pore size distribution of the main pores is narrower than the pore size distribution of the entrance (neck) diameters and where the entrances to the pores had been widened by calcination.[7] According to the pore size distribution plot, those pores with width smaller than ca. 10 nm disappear after annealing at 550°C, meanwhile pores with diameter larger than ca. 20 nm are created, resulting in an increase of the average pore width from 7.3 to 23.5 nm. It can be regarded as Ostwald ripening of the pores. The specific surface of the sample annealed at 800°C is smaller than 1 $m^2 g^{-1}$. The textural properties are crucial for the demagnesiation process as discussed below.

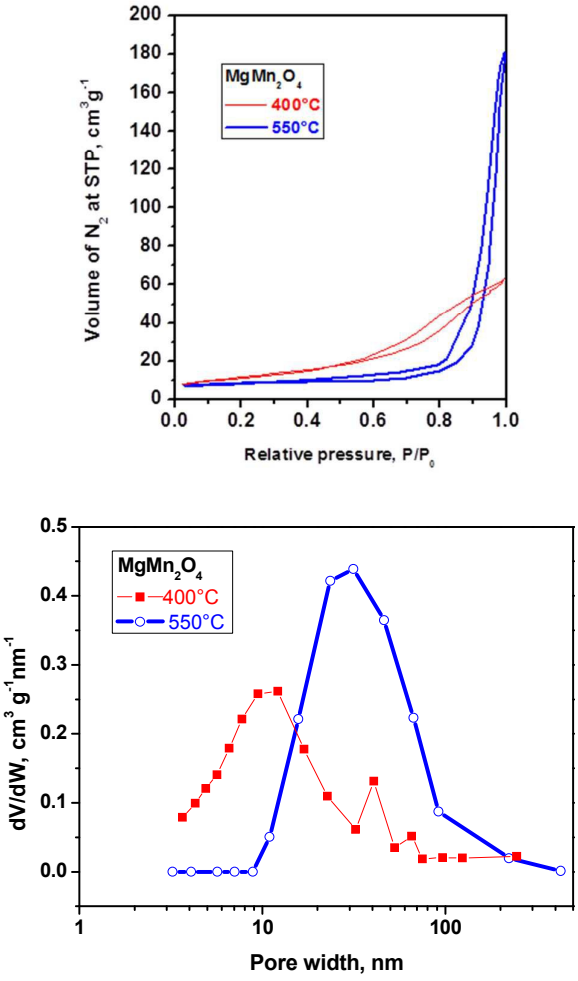

Fig. 2 Isotherms and pore size distribution for $MgMn_2O_4$ prepared at 400 and 550°C.

Table 1 Results for the analysis of the isotherms corresponding to $MgMn_2O_4$ prepared at 400 and 550°C and λ-MnO_2 obtained by chemical demagnesiation from $MgMn_2O_4$-400°C. D_{pore}= average pore diameter. V_{pore}=total pore volume. S_{BET}= specific surface area measured by BET method.

	$MgMn_2O_4$ (550°C)	$MgMn_2O_4$ (400°C)	λ-MnO_2
S_{BET}, m^2g^{-1}	25.8	85.6	196.9
V_{pore}, cm^3g^{-1}	0.29	0.20	0.38
D_{pore}, nm	23.5	7.3	7.3

3.2 Chemical demagnesiation

Magnesium can be removed from $MgMn_2O_4$ of appropriate texture by chemical methods. The acid treatment of the tetragonal spinel $MgMn_2O_4$ (s.g. $I4_1/amd$) yields the transformation to cubic λ-MnO_2 (s.g. Fd-3m, JCPDS:44-0992) where the tetragonal distortion of the lattice due to the Jahn-Teller effect in Mn(III) ions is suppressed (Fig. 3). The change of symmetry is confirmed by XRD and infrared spectroscopy. Magnesium ions are removed from tetrahedral sites of $MgMn_2O_4$ while manganese ions remain in octahedral sites, and thus λ-MnO_2 has a structure with open tunnels. Besides magnesium, manganese ions are also dissolved, and the reaction can be written as:

$MgMn_2O_4(s) \xrightarrow{HNO_3(aq)} \lambda\text{-}MnO_2(s) + MgO(aq) + MnO(aq)$

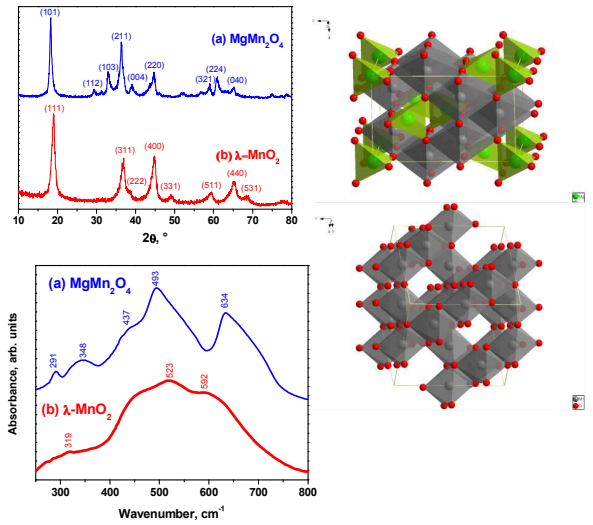

Fig. 3 X-ray diffraction patterns and FTIR spectra of (a) $MgMn_2O_4$ and (b) λ-MnO_2, where λ-MnO_2 was obtained through chemical demagnesiation of $MgMn_2O_4$ with nitric acid solution. The perspective view of $MgMn_2O_4$ and λ -MnO_2 are also shown. Mg, Mn and O atoms are shown as green, grey and red, respectively. The empty tunnels of λ-MnO_2 after the removal of Mg ions are visible.

According to ICP analysis, the resulting solid sample contains traces of magnesium (2.2% wt.). The lattice parameter of the

resulting λ-MnO_2 is a=8.07(3) Å. The unit cell of λ-MnO_2 with empty tetrahedral sites and Mn^{4+} ions is smaller than the cell of the spinel-type $LiMn_2O_4$ (a=8.24 Å) in which the tetrahedral sites are occupied by lithium ions and larger manganese(III) ions are present.

In the FTIR spectra, at least five bands are observed in the range between 250 and 800 cm^{-1} for tetragonal $MgMn_2O_4$. These bands are shifted to higher frequencies in comparison with the hausmanite (Mn_3O_4) normal tetragonal spinel, and this fact is consistent with the lighter mass of Mg^{2+} and the shorter distance of the magnesium-oxygen bond. The removal of magnesium involves changes in the FTIR spectra. The high local symmetry of the cubic λ-MnO_2 and the vacancies in the tetrahedral sites are reflected in the observation of fewer bands. The spectrum of λ-MnO_2 is consistent with the literature and the predicted three infrared-active vibrations ($^3F_{1u}$).[8]

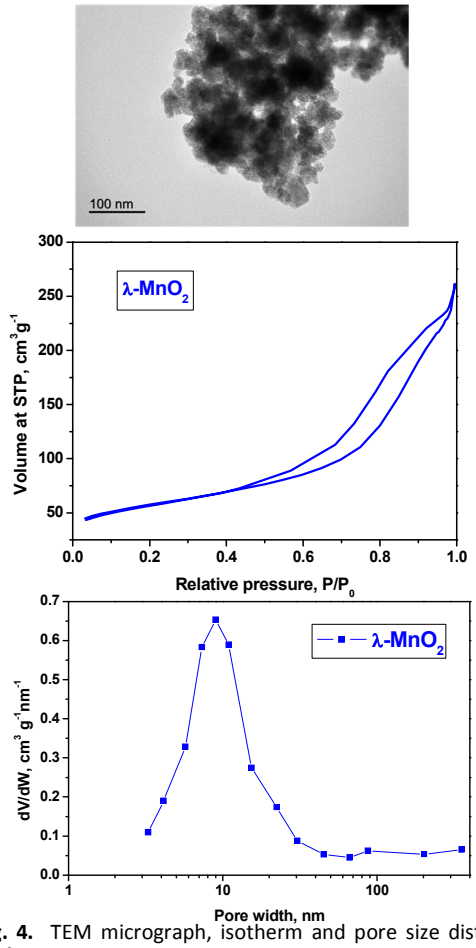

Fig. 4. TEM micrograph, isotherm and pore size distribution for λ-MnO_2.

On the other hand, the acid treatment of $MgMn_2O_4$ annealed at 400°C yields to λ-MnO_2 where more mesopores with width between ca. 4 and 30 nm are formed, the total pore volume increases and the average pore radius remains unchanged (Fig. 4 and Table 1). The resulting λ-MnO_2 sample possesses higher specific surface area (S_{BET}=196.9 m^2g^{-1}) than pristine $MgMn_2O_4$ (S_{BET}=85.6 m^2g^{-1}).

In contrast to $MgMn_2O_4$ obtained at 400°C, the sample annealed at 550°C and treated with acid solution under the same experimental conditions does not yield single-phase λ-MnO_2, the pristine tetragonal structure is preserved and only a small amount of cubic λ-MnO_2 is obtained (see SEI). This fact involves that the particle surface and porosity that is in contact with the acid solution are key parameters to achieve the chemical demagnesiation. For the sample prepared at 550°C, the surface of the particles in contact with the acid solution is smaller and the diffusion path of ions in the particles is longer.

3.3 Effect of thermal annealing on λ-MnO_2

Another adequate method to characterize manganese dioxide is by using thermal analysis. In addition, the electrode materials used in batteries often are thermally treated to obtain dry and high-crystallinity powders. The DSC and XRD (Fig. 5) results reveal that the as-prepared λ-MnO_2 is not stable with respect to thermal annealing. This involves that λ-MnO_2 with high crystallinity and large crystallite size could not be prepared by thermal treatment, because it is a metastable form of MnO_2. And this fact may limit its potential use in non-aqueous batteries. In the DSC curve, there is an endothermic and broadened peak at about 60-250°C. The XRD patterns only show progressive loss of crystallinity in the λ-MnO_2 phase up to 300°C. An exothermic peak is observed at about 340°C, while the occurrence of the phase Mn_5O_8 ($Mn_2^{2+}Mn_3^{4+}O_8$) is detected at 400°C (C2/m, a=10.36(5) Å, b=5.72(1) Å, c=5.69(3) Å, β=110.53°, JCPDS:39-1218) and the reflections of λ-MnO_2 disappear.

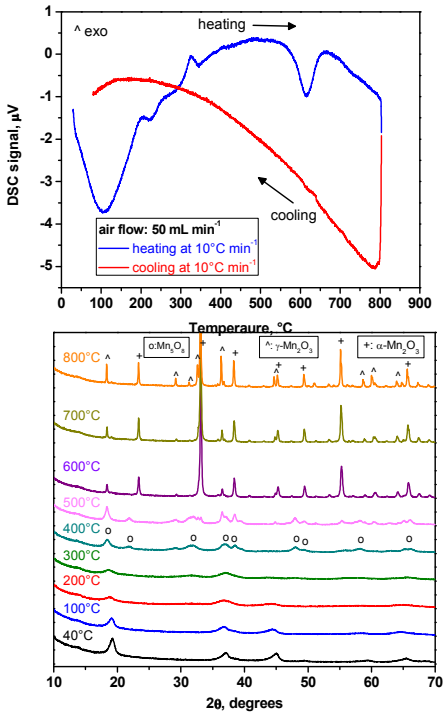

Fig. 5. DSC curves for heating and cooling of λ-MnO_2 under air-flow, and *in-situ* recorded XRD patterns for the annealing of λ-

MnO_2 in air atmosphere. Endothermal is downward and exothermal is upward.

After annealing at 600-800°C, the observed reflections are ascribed to cubic bixbyite α-Mn_2O_3 ($P2_13$, a=9.42(2) Å, JCPDF:41-1442) and tetragonal γ-Mn_2O_3 ($I4_1/amd$, a=5.74(1) Å, c=9.403(4) Å). Although Mn_3O_4 and $MgMn_2O_4$ also crystallize in the same space group than γ-Mn_2O_3, the positions of the Bragg reflections and the calculated lattice parameters agree better with the last phase. The endothermic peak placed at ca. 614°C is ascribed to the formation of bixbyite α-Mn_2O_3.[9] This last endothermic peak was not observed in the DSC experiment recorded under Ar-flow, and the XRD pattern of the sample retrieved from the DSC experiment did not exhibit reflections of orthorhombic α-Mn_2O_3, only the tetragonal phase was detected (see SEI).

3.4 Electrochemical demagnesiation and cycling of $MgMn_2O_4$ in aqueous solution

In an attempt to remove magnesium from $MgMn_2O_4$, prepared at 400°C (LT) and 800°C (HT), by electrochemical methods an aqueous solution of magnesium nitrate was used as electrolyte (Fig. 6). During the first sweep, the voltage was increased from the open circuit voltage (OCV) to 3.0 V vs. Ag/AgCl, then the cell was relaxed for one minute, and finally a second anodic sweep was imposed from OCV to 3.0 V at the same scan rate. Decomposition of the electrolyte solution and gas evolution also took place at these anodization voltages in competition against the oxidation of $MgMn_2O_4$ and decreasing the coulombic efficiency. Two anodic peaks are observed between 1.0 and 2.5 V which are ascribed to the oxidation of Mn(III) to Mn(IV) (similarly to the deinsertion of lithium from $LiMn_2O_4$), and at higher voltage oxygen evolution is observed. The capacity of the first charge process is 112.6 mAh g^{-1} for HT and 296 mAh g^{-1} for LT. The peaks between 1.4 and 2.1 V are not observed during the second anodic sweep and the capacity of this second charge process is 59 mAh g^{-1} for HT and 45 mAh g^{-1} for LT. The *ex-situ* XRD patterns of both HT and LT-$MgMn_2O_4$ electrochemically oxidized electrodes show that the pristine structure of $MgMn_2O_4$ is preserved and the unit cell is only slightly contracted (a=b=5.715(5) Å, c=9.3154(9) Å, Vol.=304.23 $Å^3$). The cubic spinel λ-MnO_2 is not formed. The oxidation of manganese(III) under these experimental conditions apparently does not involve the significant extraction of magnesium from the inner part of the particle, and the electrochemical reaction mainly takes place at the particle surface, similarly to an electrochemical capacitor.

It is important to find suitable conditions for the demagnesitation process. The upper voltage limit of the working electrode and the parasitic reactions need to be controlled. In contrast to the voltammetry results, the oxidation of LT-$MgMn_2O_4$ under constant current (galvanostatic method) and continuously flowing Ar through the aqueous solution yields to the whole extraction of magnesium and formation of λ-MnO_2 (Fig. 7):

$$MgMn_2O_4(s) \rightarrow \lambda\text{-}MnO_2(s) + Mg^{2+}(aq) + 2e^-$$

A plateau is observed at ca. 1.4 V which involves demagnesiation from $MgMn_2O_4$ and finally formation of λ-MnO_2 (Fig. 7). The limited contribution of irreversible decomposition of electrolyte solution at this plateau cannot be discarded. If one compares Fig. 6 and Fig. 7, it is deduced that besides the imposed voltage limit, Ar-flow and oxygen removal from the electrolyte solution also can contribute to improve the stability of the electrode material in aqueous cell and to decrease the cell polarization, like other authors previously found in other aqueous batteries.[10] We can speculate that the continue Ar-flow avoids some parasitic reactions and self-discharge which are related to the presence of O_2 dissolved in the solution. Thus, if an oxidation is being performed at the positive electrode ($MgMn_2O_4$) in aqueous solution, the dissolved O_2 can be electrochemically reduced at the negative electrode (Pt) or, alternatively, H_2 can be formed at the Pt electrode. It may be that the oxygen reduction produces compounds (e.g. H_2O_2) which chemically react at the working electrode and also reduce the activity of the Pt electrode. In contrast, the Ar-flow suppresses these irreversible reactions and improves the overall electrochemical performance.

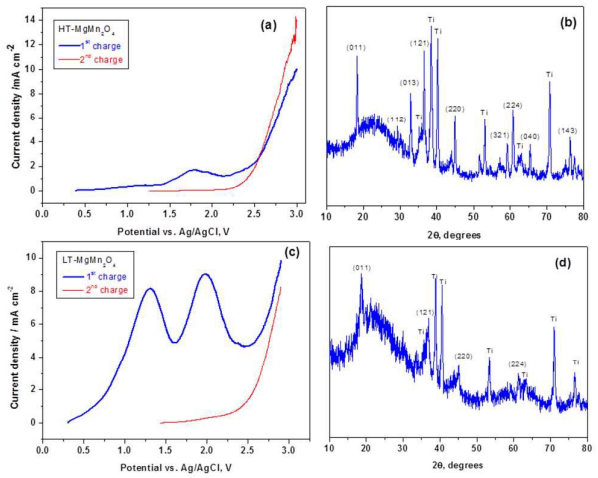

Fig. 6. Voltammetry results (two consecutive anodization processes) for trying to remove magnesium from $MgMn_2O_4$ prepared at 400 (LT) and 800°C (HT). (a) Intensity-voltage plot for HT. (b) Resulting XRD for HT. (c) Intensity-voltage plot for LT. (d) Resulting XRD for LT. Scan rate: 5 mV/s. The reflections of the Ti substrate are marked, and the hump at 15-30°/2θ is also due to the Ti substrate.

In addition, we observed that after cycling voltammetry of λ-MnO_2 in an aqueous solution of magnesium nitrate, the cubic structure of λ-MnO_2 is transformed into the tetragonal structure of $MgMn_2O_4$ (Fig. 8). On the other hand, the lithiation of λ-MnO_2 by cyclic voltammetry in an aqueous solution containing lithium nitrate drives to an expansion of the cubic cell (a=8.3(2) Å) up to nearly the value corresponding to $LiMn_2O_4$ (Fig. 8).

The reversible lithiation/delithiation of the cubic $Li_xMn_2O_4$ is well known in the literature. However, the reversible magnesiation/demagnesiation process starting from tetragonal $MgMn_2O_4$ is less known, and this is the first time that single-phase λ-MnO_2 has been prepared by chemical and electrochemical demagnesiation and then reinserted by electrochemical methods. This find suggests that the manganese oxides may be effectively used in magnesium-ion batteries. Moreover, all these results

evidence that the magnesiation/demagnesiation is a reversible process for the spinel-type $Mg_xMn_2O_4$ in spite of the tetragonal distortion in the lattice. The divalent charge of the Mg(II) ion theoretically can double the coulombic capacity in comparison with systems based on lithium-ion.

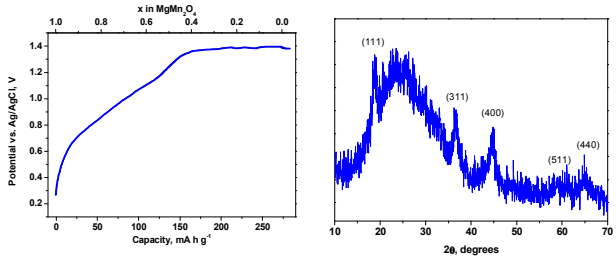

Fig. 7. Galvanostatic charge of LT-$MgMn_2O_4$ in aqueous battery and *ex-situ* XRD of the charged electrode. The Miller indexes of the cubic λ-MnO_2 phase are shown.

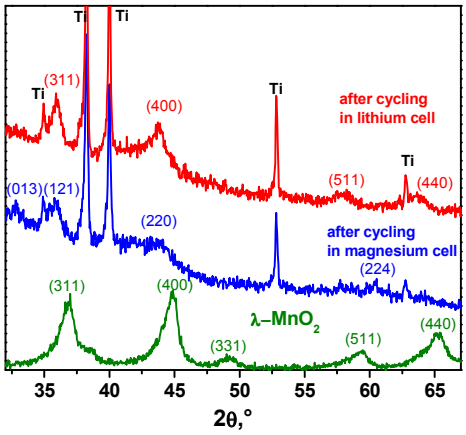

Fig. 8. E*x-situ* XRD patterns for the cycled electrodes of λ-MnO_2 in aqueous electrolyte containing lithium and magnesium salts. The Miller indexes of the cubic and tetragonal phases are shown.

For galvanostatic cycling in aqueous cell, the initial reversible capacity of $MgMn_2O_4$ is ca. 150 mAh g^{-1}, and this value is higher than those reported for $LiMn_2O_4$ in aqueous lithium electrolyte which are typically below 130 mAh g^{-1} (Fig. 9).[11] Probably, the electrostatic interactions between Mg^{2+} ions and water molecules enhance the reversible electrochemical activity of the manganese oxides.[12] However, electrolyte decomposition and the deterioration of the lattice structure, mostly due to the Jahn-Teller distortion, may contribute to the capacity fade upon cycling. Further improvement of the electrochemical system would be needed before commercial application.

Aqueous magnesium-ion batteries may be superior to aqueous lithium-ion batteries in terms of specific capacity, economic cost, sustainability and environmental issues.

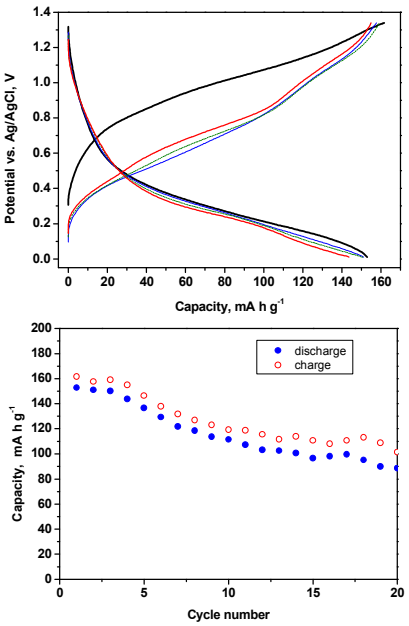

Fig. 9. Results of the galvanostatic cycling for LT-$MgMn_2O_4$ in aqueous cell. Current intensity: 60 μA.

3.5 Electrochemical cycling of $MgMn_2O_4$ in non-aqueous solution

Another strategy concerns the use of non-aqueous electrolytes which may deliver higher voltages, higher capacities and prolonged cycling. Non-aqueous electrolyte solutions made of magnesium salts such as $Mg(ClO_4)_2$ and carbonates solvents such as PC, EC and DEC do not allow the reversible dissolution/deposition of magnesium from/on metallic Mg electrode. Mg in AN solution is passivated by spontaneous formation of surface films and, although magnesium dissolution may occur by breakdown of this surface film, this type of electrolyte solutions do not allow reversible release of magnesium ions from the Mg metal electrode. It is due to the reactivity of AN, which its reduction forms a surface film that covers Mg electrode leading to the rise of the cell impedance.[5] Solutions of Grignard compounds in THF exhibit better reversibility for magnesium deposition, but corrosion of the current collectors and battery case use to happen with these solutions.

We have made and tested non-aqueous magnesium-ion batteries with $MgMn_2O_4$ as positive electrode versus V_2O_5 as negative electrode and using non-aqueous and non-corrosive electrolyte solution (Fig. 10). The reversible capacity refereed to the mass of $MgMn_2O_4$ is about 120 mAh g^{-1}. The results show that magnesium ions are reversible inserted/desinserted in both the positive and the negative electrode and the concept of a veritable magnesium-ion battery can be viable. Since the operation voltage of the battery shown in Fig. 10 is not satisfactory, then a problem to overcome is to use positive electrode materials of higher voltage and negative electrode materials of lower voltage for achieving a higher voltage in the whole battery.

The ex-situ XRD patterns recorded at selected states of the first charge process of $MgMn_2O_4$ obtained at 800°C show that the

structure of $MgMn_2O_4$ is preserved during the extraction of magnesium (see ESI). Cubic λ-MnO_2 is not formed, and there is not a clear explanation of this fact. There is a contraction of the lattice in the direction of the c-axis and the tetragonal lattice is slightly contracted. One may think that the crystallinity of $MgMn_2O_4$-800°C hinders the formation of λ-MnO_2. However, we have checked that, the tetragonal structure of $MgMn_2O_4$-400°C is also preserved at the end of the first electrochemical charge (280 mAh g^{-1}) in non-aqueous cell (see ESI), and also a contraction of the cell is observed (a=5.72(3) Å, c=9.21(3) Å, Vol.= 301.26 $Å^3$). These results indicate that the cubic phase of manganese dioxide is only stabilized in aqueous solution and not in EC-DEC solvents. Probably water molecules are incorporated into the framework of λ-MnO_2 during its electrochemical cycling in aqueous solution. On the other hand, in the case of non-aqueous solvent probably the lack of water in the oxide improves the cycling stability of the tetragonal phase.

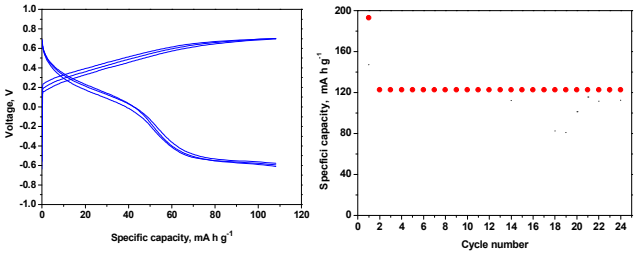

Fig. 10 Typical voltage-capacity curves and capacity vs. cycle number plots for a magnesium-ion battery in a non-aqueous and non-corrosive electrolyte solution. Positive electrode: $MgMn_2O_4$-400°C. Negative electrode: commercial V_2O_5 (used in excess, m_+/m_-=0.53). Electrolyte solution: 0.5 M $Mg(ClO_4)_2$ in EC:DEC. Current intensity: 10 μA.

The effective use of $MgMn_2O_4$ as active material for the positive electrode in a magnesium-ion battery, in turn, requires appropriate materials that can be used like negative electrode. These negative electrode materials should have high specific capacity and operate within certain voltage window. V_2O_5 and MnO_2 operate in a voltage which is too high. Alloys and compounds containing magnesium-alloying elements should be explored.

4. Conclusions

We have observed that magnesium can be reversibly removed from $MgMn_2O_4$ by chemical and electrochemical methods and using aqueous and non-aqueous media, and even the cubic phase λ-MnO_2 can be obtained in aqueous solution, but the textural properties and the experimental conditions have to be carefully selected. The chemical demagnesiation is easier for particles prepared at low temperature, with small particle size and having many mesopores with diameter smaller than ca. 20 nm. This mechanism of ion extraction is different from $Li_xMn_2O_4$, where the spinel-type structure is always cubic for 0<x<1. The results show that it may be possible to develop a veritable magnesium-ion battery based on non-corrosive electrolytes solutions. Although the use of deoxygenated aqueous solutions also is promising, the electrochemical cycling of $MgMn_2O_4$ seems to be more stable in non-aqueous electrolyte based on carbonates solvents. In non-aqueous electrolyte, the charge process (demagnesiation) of $MgMn_2O_4$ yields to a contraction of the tetragonal lattice in the direction of the c-axis, and the phase λ-MnO_2 is not formed.

Acknowledgements

The authors would like to greatly acknowledge MICINN (MAT2011-22753 and MAT2014–56470-R) and Junta de Andalucía project FQM-7206 for financial support. The instruments for FTIR, ICP and TEM were provided by SCAI (UCO Central Service for Research Support).

Notes and references

1 A. Luntz, *J. Phys. Chem. Lett.*, 2015, **6**, 300; M. Armand and J.M. Tarascon, *Nature*, 2008, **451**, 652 ; P. Novák, R. Imhof and O. Haas, *Electrochim. Acta*, 1999, **45**, 351; P.G. Bruce, F. Krok, V.C. Gibson and K. Tavakkoli, *J. Mater. Chem.*, 1991, **1**, 705.

2 M.M. Huie, D.C. Bock, E.S. Takeuchi, A.C. Marschilok and K.J. Takeuchi, *Coord. Chem. Rev.*, 2015, **287**, 15; C. Kim, P.J. Phillips, B. Key, T. Yi, D. Nordlund, Y.S. Yu, R.D. Bayliss, S.D. Han, M. He, Z. Zhang, A.K. Burrell, R. F. Klie and J. Cabana, *Adv. Mater.*, 2015, **27**,3377; J.S. Kim, W.S. Chang, R.H. Kim, D.Y. Kim, D.W. Han, K.H. Lee, S.S. Lee and S.G. Doo, *J. Power Sources*, 2015, **273**, 210; J. Muldoon, C.B. Bucur and T. Gregory, *Chem. Rev.*, 2014, **114**, 11683; P. Saha, M.K. Datta, O.I. Velikokhatnyi, A. Manivannan, D. Alman and P.N. Kumta, *Prog. Mater Sci.*, 2014, **66**, 1.

3 C. Ling , F. Mizuno , *Chem. Mater.*, 2013, **25** , 3062.

4 R. Zhang, T.S. Arthur, C. Ling and F. Mizuno, *J. Power Sources*, 2015, **282**, 630.

5 R. Mohtadi and F. Mizuno, *Beilstein J. Nanotechnol.*, 2014, **5**, 1291; O. Mizrahi, N. Amir, E. Pollak, O. Chusid, V. Marks, H. Gottlieb, L. Larush, E. Zinigrad and D. Aurbach, *J. Electrochem. Soc.*, 2008, **155**, A103; Z. Lu, A. Schechter, M. Moshkovich and D. Aurbach, *J. Electroanal. Chem.*, 1999, **466**, 203.

6 S. Yagi, A. Tanaka, Y. Ichikawa, T. Ichitsubo and E. Matsubara, J. Electrochem. Soc., 2013, **160**, C83.

7 M. Kruk, E. B. Celer, J. Matos, S. Pikus and M. Jaroniec, *J. Phys. Chem. B*, 2005, **109**, 3838; M. Thommes, *Chem-Ing-Tech*, 2010, **82**, 1059.

8 C.M. Julien, M. Massot and C. Poinsignon, *Spectrochim Acta A,* 2004, **60**, 689.

9 C. Hunter, *J. Solid State Chemistry*, 1981, **39**, 142; N. Wang, X. Cao, L. He, W. Zhang, L. Guo, C. Chen, R. Wang and S. Yang, *J. Phys. Chem. C*, 2008, **112**, 365; C. Wang, Y. Zhai, X. Wang and M. Zeng, *Front. Chem. Sci. Eng.*, 2014, **8**, 471.

10 J.Y. Luo, W.J. Cui, P. He and Y.Y Xia, *Nat Chem*, 2010, **2**, 760; P. He, J.L. Liu, W.J. Cui, J.Y. Luo, and Y.Y. Xia, *Electrochim. Acta*, 2011, **56**, 2351; M. Zhao, B. Zhang, G. Huang, H. Zhang, and X. Song, *J. Power Sources*, 2013, **232**, 181.

11 Y. Wang, L. Chen, Y. Wang and Y. Xia, *Electrochim. Acta*, 2015, **173**, 178; S. Liu, S.H. Ye, C.Z. Li, G.L. Pan and X.P. Gao, *J. Electrochem. Soc.*, 2011, **158**, A1490; L. Liu, F. Tian, M. Zhou, H. Guo, X. Wang, *Electrochim. Acta*, 2012, **70**, 360; W.

Li, J. R. Dahn, and D. S. Wainwright, *Science*, 1994, **264**, 1115; H. Manjunatha, G.S. Suresh and T. V. Venkatesha, *J. Solid State Electrochem*., 2011, **15**, 431; G.X. Wang, S. Zhong, D.H. Bradhurst, S.X. Dou and H.K. Liu, *J. Power Sources*, 1998, **74**, 198.

12 K.W. Nam, S. Kim, S. Lee, M. Salama, I. Shterenberg, Y. Gofer, J.S. Kim, E. Yng, C.S. Park, J.S. Kim, S.S. Lee, W.S. Chang, S.G. Doo, Y.N. Jo, Y. Jung, D. Aurbach and J.W. Choi, *Nano Lett.,* DOI: 10.1021/acs.nanolett.5b01109.